Key Points:
- A Na lidar's 29-year observations show a dropping of the upper atmosphere boundary between mesosphere and thermosphere (mesopause)
- The mesopause temperature has been cooling since 1990 at the rate of about 2 degree for every ten years, but becomes less significant after 2000
- The mesopause variations, including temperature and height, in summer is more sensitive to solar activities than the winter mesopause

Correspondence to:
T. Yuan,
titus.yuan@usu.edu

The Long-Term Trends of Nocturnal Mesopause Temperature and Altitude Revealed by Na Lidar Observations Between 1990 and 2018 at Midlatitude

Tao Yuan[1,2] ID, **S. C. Solomon[4]** ID, **C.-Y. She[3]** ID, **D. A. Krueger[3]**, and **H.-L. Liu[4]** ID

[1]Center for Atmospheric and Space Sciences, Utah State University, Logan, UT, USA, [2]Physics Department, Utah State University, Logan, UT, USA, [3]Physics Department, Colorado State University, Ft. Collins, CO, USA, [4]National Center for Atmospheric Research, Boulder, CO, USA

Abstract The mesopause, a boundary between mesosphere and thermosphere with the coldest atmospheric temperature, is formed mainly by the combining effects of radiative cooling of CO_2, and the vertical adiabatic flow in the upper atmosphere. A continuous multidecade (1990-2018) nocturnal temperature data base of an advanced Na lidar, obtained at Fort Collins, CO (41°N, 105°W), and at Logan, UT (42°N, 112°W), provides an unprecedented opportunity to study the long-term variations of this important atmospheric boundary. In this study, we categorize the lidar-observed mesopause into two categories: the "high mesopause" (HM) above 97 km during nonsummer months, mainly formed through the radiative cooling, and the "low mesopause" (LM) below 92 km during nonwinter months, generated mostly by the adiabatic cooling. These lidar observations reveal a cooling trend of more than 2 K/decade in absolute mesopause temperature since 1990, along with a decreasing trend in mesopause height: The HM is moving downward at a speed of ~ 450 ± 90 m/decade, while the LM has a slower downward trend of ~ 130 ± 160 m/decade. However, since 2000, while the height trend (- 470 ± 160 m/decade for the HM and 150 ± 290 m/decade for the LM) is consistent, the temperature trend becomes statistically insignificant (- 0.2 ± 0.7 K/decade and -1 ± 0.9 K/decade for the HM and the LM, respectively). A long-term study by Whole Atmosphere Community Climate Model with thermosphere and ionosphere extension (WACCM-X) also indicated the similar mesopause changes, mostly caused by stratosphere-lower mesosphere cooling and contraction.

1. Introduction

The thermal radiative balance in the mesosphere and lower thermosphere (MLT) is achieved by contributions from the absorption of the ultraviolet (UV) spectrum in solar radiation, chemical heating from exothermic reactions, radiative cooling of CO_2 and adiabatic heating, or cooling processes due to the vertical flow in global atmospheric circulation (Brasseur & Solomon, 2005; Roble, 1995). During the night, when the heating by solar UV radiation is turned off, along with the exothermic reactions that are associated with photochemistry and photoionization, the MLT thermal budget is then mostly controlled by the radiative cooling and the adiabatic heating/cooling. The mesopause, where the minimum temperature in the terrestrial atmosphere occurs, is formed in this conjunction area, and marks the genuine boundary between the mesosphere and thermosphere. The seasonal variation of zonal mean flow in the stratosphere and lower mesosphere, caused by the combination of seasonal change of meridional temperature gradient in stratosphere and Coriolis force, alters the gravity wave filtering scheme and leads to the seasonal variation of gravity wave dissipation and drag in the MLT region (Holton, 1983). This, combined with the summer pole to winter pole circulation, results in the seasonal variations of the vertical adiabatic flow: a down-welling flow in winter hemisphere and an up-welling flow in the summer hemisphere. The adiabatic process associated with such vertical motions enhances the departure from radiative equilibrium and forms a cold summer mesopause at low altitudes in summer below the radiative mesopause at about 100 km, while the winter mesopause occurs at higher altitudes above 100 km and is still mainly controlled by radiative balance. Thus, the depth of the winter mesopause reflects the combined effects of radiative cooling and adiabatic warming, while the summer mesopause reflects the combined effects of both radiative and adiabatic cooling. Such mesopause temperature and height oscillations between the summer and winter
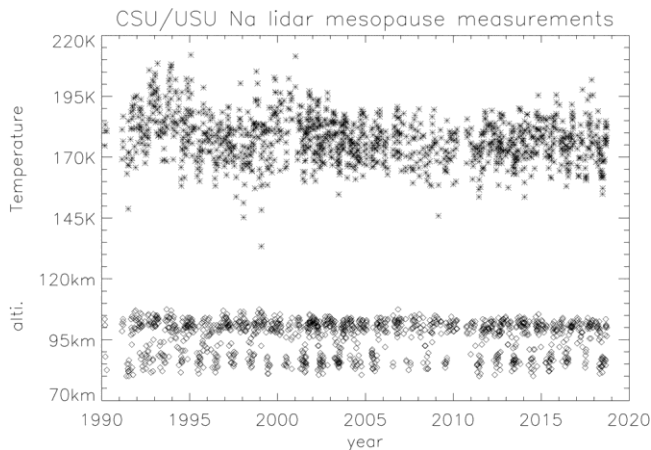
Figure 1. The Na lidar-measured mesopause temperatures (asterisks) and mesopause heights (diamonds) between 1990 and 2018 at Colorado State University (1990 to March 2010) and Utah State University (September 2010 to present).

have been well documented by ground-based lidar and spaceborne observations (She et al., 1993; She & von Zahn, 1998; von Zahn et al., 1996; Xu et al., 2007; Yuan et al., 2008).

As various experimental and modeling studies have shown over the past few decades, the increasing levels of CO_2 throughout the atmosphere, and O_3 depletion in the stratosphere, have considerable impact on long-term variation of the MLT region (Akmaev et al., 2006; Bremer & Peters, 2008). Since Roble and Dickinson (1989) predicted the resulting cooling in the upper atmosphere because of the increasing radiative cool-ing by CO_2, many experimental studies, involving various technologies and instruments, have been conducted to reveal the magnitude of the long-term temperature trend in the MLT (Beig, 2011; Laštovička, 2012; Laštovička & Bremer, 2004, and references within). Although the cooling in the MLT is confirmed, these results have been inconsistent with respect to the magnitude of the cooling trend. Recently, based on 25 years of Na lidar data taken at Colorado State University (41°N, 105°W) and Utah State University (42°N, 112°W) from 1990 to 2014, She et al. (2015) revealed an overall cooling trend in the mesopause region (0.64 ± 1.0 K/decade at 85 km, increasing to a maximum of 2.8 ± 0.6 K/decade between 91 and 93 km). An exception is the insignificant warming trend above 103 km, most likely due to the combined effect of stratospheric con-traction and large positive temperature gradient in the lower thermosphere.

While the experimental observations report trend values at each geometric altitude, model studies on long-term trend tend to conduct investigations at pressure heights to eliminate the ambiguity due to atmospheric contraction. Thus, they are able to focus on long-term effects in the upper atmosphere by the specific mechanism, such as CO_2 accumulation and solar cycle effects. Such differences in data processing make the validation work on these results, between observational and numerical approaches, very challenging. On the other hand, the mesopause, a specific natural atmospheric boundary with zero vertical temperature gradient, can serve as a reliable natural geographic level for such investigation. For example, the long-term trend of its height could provide the unique insight of magnitude of the stratosphere and mesosphere con-traction, while the trend of winter mesopause temperature could reflect the long-term change of CO_2 radiative cooling.

In this paper, we are investigating the long-term trends of mesopause height and temperature based on the nocturnal temperature observations by a Na temperature/wind lidar obtained at the two nearby stations (Colorado State University [CSU] and Utah State University [USU] that are ~580 km apart) between 1990 and 2018. Because of the similar geographical locations of the lidar operations, we combine the data from the two sites, allowing for a single continuous multidecadal time series (She et al., 2015). To demonstrate the continuity of this data set, we calculate the annual mean temperature of 2006 (CSU observations) and that of 2012 (USU observations) in the mesopause region, symmetric about the solar minimum in 2009. As expected, this simple calculation shows very similar annual mean (184.0 K for 2006 and 184.2 K for 2012) and standard deviations (8.2 K for 2006 and 7.4 K for 2012) of the lidar data taken at these two loca- tions. Due to the aforementioned different mechanisms of summer and winter mesopause, we categorize the lidar mesopause data into two groups, based upon their altitudes and season of occurrence, and analyze their individual long-term trend separately in section 2. These experimental results are compared with the trend simulations using the Whole Atmosphere Community Climate Model with thermosphere and iono- sphere extension (WACCM-X; Liu et al., 2018; Solomon et al., 2018) in section 3, followed by discussion and conclusions in sections 4 and 5.

2. The Na Lidar Measured Mesopause

The Na lidar measures neutral temperature and wind in the mesopause through the detection of Doppler broadening and Doppler shift in the fluorescence spectrum of atomic Na atoms in MLT (Krueger et al., 2015). Figure 1 shows the variation of mesopause temperature and height from 1990 to 2018 (the lidar data after summer 2010 are taken at USU station). Each data point represents a nightly averaged lidar
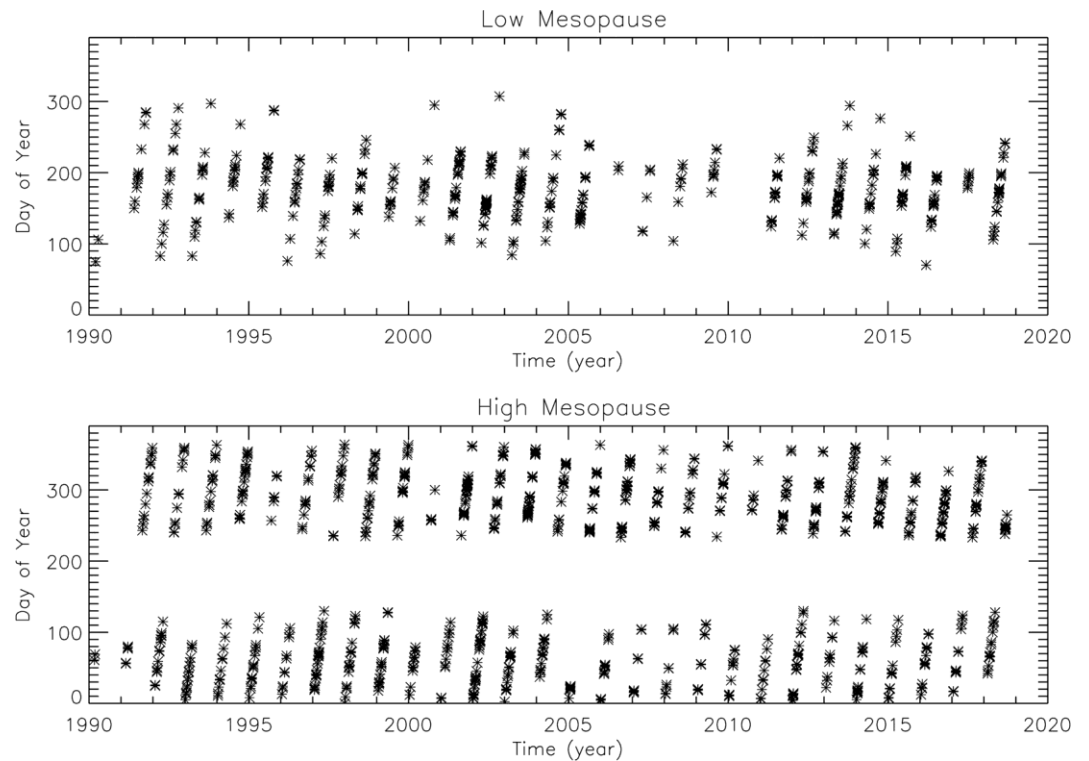
Figure 2. Day-of-year for the lidar-measured (top) nonwinter low mesopause and (bottom) nonsummer high mesopause. Those mesopause occurring below 92 km between March and October are categorized as low mesopause; those above 97 km between August and February of the coming year are categorized as high mesopause.

measurement of no less than 4 hr. The lidar data, total of 1,388 nights of such observations, are also smoothed by sliding a 2-km full width at half maximum (FWHM) Hanning window in the vertical direction in the temperature retrieval process, and later interpolated onto a grid with 0.5-km interval. The lidar-measured temperatures with uncertainty larger than 3 K are discarded. Here the mesopause is identified by finding the minimum temperature in the nightly averaged lidar temperature profile between 75 and 110 km with vertical gradient less than 2 K/km. As indicated by the figure, the day-to-day variability of mesopause temperature is fairly large, with standard deviation of ~9.5 K and mean value of

~177.6 K. The episodic warming due to Mt. Pinatubo eruption (She et al., 2009) appears to affect mesopause temperature in the early 1990s. However, a recent investigation has demonstrated that the lingering effect by Mt. Pinatubo eruption should have died out by 1999 in the mesopause region (She et al., 2015). Thus, its impact on later data is marginal. More importantly, the figure also shows that the variation of mesopause height is dominated by the summer-winter oscillation and does not show any sign of effects by the aforementioned episodic warming. Based on the figure, the mesopause height data can be clearly grouped into two categories: one above 95 km and one below 95 km. We, thus, categorize the mesopause that occurs above 97 km as "high mesopause" (HM) and the mesopause that forms below 92 km as "low mesopause" (LM). In addition, we focus our investigation on HM during nonsummer months and LM during nonwinter months. This is because, while the mesopause formation is controlled by both the adiabatic mean flow and thermal radiation balance, the occurrence rates of HM in summer and LM in winter are very low in summer and winter, respectively, due to the dominance of either mechanism in these two seasons. Overall, there are 388 nights in LM and 824 nights in HM, total of 1,212 nights in this data set are identified. Note that there are only 106 nights (less than 8%) when the mesopause height is between 92 and 97 km. We plot the day-of-year distribution of these two groups of mesopause in Figure 2, which indicates that the "LM" mostly occurs between day-of-year 100 and day-of-year 220 (April to early August, but concentrated in summer), while the "HM" is formed in fall through early spring (from late August to early April). Thus, the LMs can be seen as mostly controlled by the adiabatic cooling and the HMs are dominated by the radiative cooling process. Based on this data set, the mean temperatures are
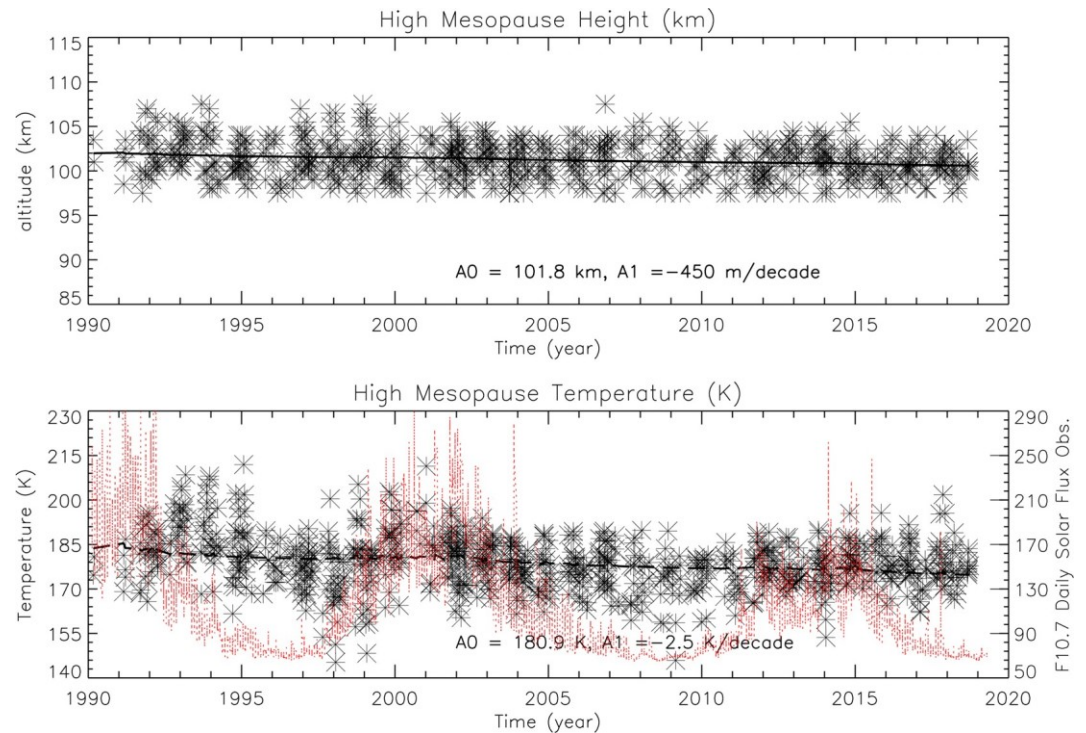
Figure 3. The long-term variations of (top) mesopause height and (bottom) temperature trend of the lidar-measured nonsummer high mesopause, along with their constant, A0, and linear (A1) terms derived from the trend regression.

about 174 and 179 K for LM and HM, respectively. The standard deviation is about 9 K for both groups of mesopause. On the other hand, the mean mesopause height for the two groups is 86 and 101 km, with standard deviation of 2.6 and 2.0 km.

$$M_{fit}(t) = M_0 + M_1 \cdot t + M_2 \cdot S_{daily}(t) \tag{1}$$

The linear regression algorithm that we utilize (equation (1)) to derive the long-term trend from the lidar data includes three terms: the constant (the initial value), M_0; linear trend, M_1; and the solar response term M_2. S_{daily}, in K/SFU or m/SFU (depending on whether we fit temperature or height), is the daily F10.7 solar flux downloaded from http://www.spaceweather.ca/solarflux/sx-en.php. Since we split the mesopause into the two afore mentioned categories that belong to different parts of the year (the LM occurs mostly in summer, and the temperature above 97 km of the HM in the mesopause region also has small seasonal variation; She & von Zahn, 1998), we ignore the effects due to seasonal, annual, and semiannual variations in the regression algorithm. The episodic warming effect is also excluded from the regression fit function. Because of their distinct formation mechanisms, we fit the lidar measured LMs and HMs separately to inves- tigate their trend individually.

The regression on height of the HMs (see Figure 3 top) shows a downward trend with the speed of ~450 ± 90 m/decade. The almost straight line of the $M_{fit}(t)$ indicates the limited impact by solar flux on HM height (M_2 = 1 m/SFU and is less than the fitting uncertainty, one sigma). At the same time, the temperature of the HM (see Figure 3 bottom) has a cooling trend of 2.5 ± 0.4 K/decade. The LM also demonstrates a down- ward trend at about ~130 ± 160 m/decade (Figure 4 top). But, considering that the fitting uncertainty (one sigma) is slightly larger than the trend, the LM either stays almost around a constant altitude or moves down at a slower pace than that of the HM. Intriguingly, the height of LM is much more sensitive to solar flux (M_2 = − 120 ± 30 m/SFU) than that of the HM, which makes the fitting line become a curve compared to the straight line of HM height fitting. Note that the height of LM is slightly anticorrelated to the F10.7 solar flux; that is, it is lower during solar max condition. The temperature trend of LM is also a cooling trend with similar magnitude (2.3 ± 0.5 K/decade) to that of the HM. This is in good accord with another long-term trend study at middle latitude by lidar observations and model simulations on the summer mesosphere
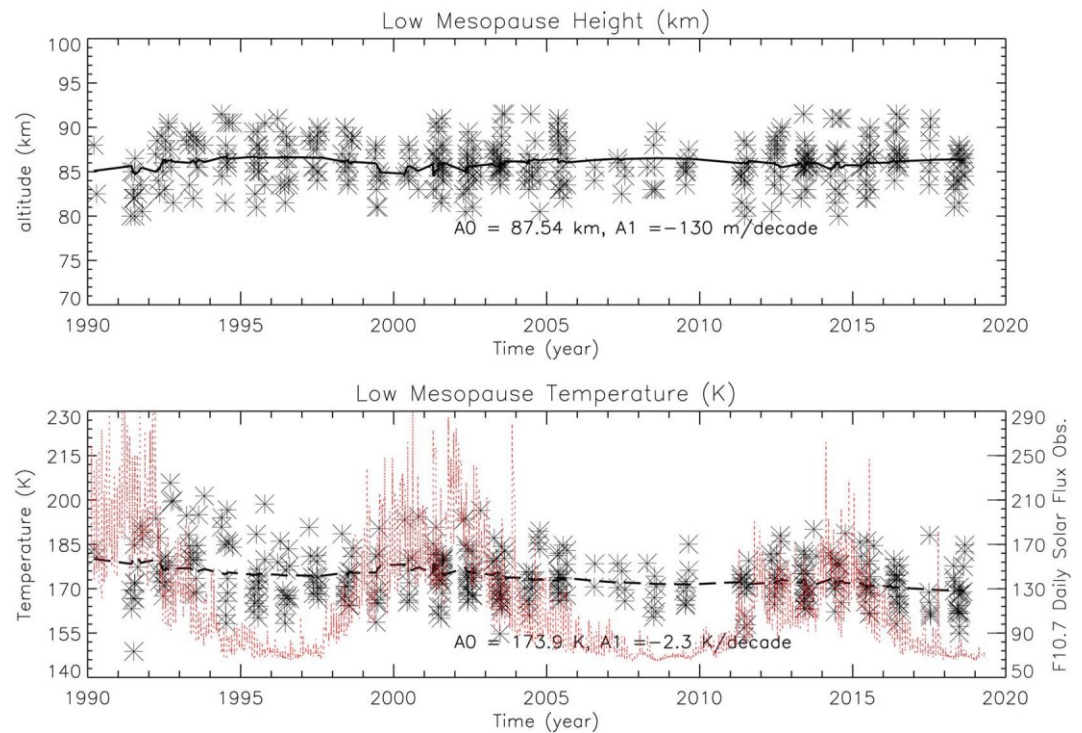
Figure 4. Same as Figure 3 but for the results of the lidar-measured nonwinter low mesopause.

region (Berger & Lübken, 2011), which found that the cooling in the summer mesosphere is 2-4 K/decade. The larger uncertainties of the LM results, compared with those of the HM, are due to relatively shorter time window for its occurrence (~100 days), leading to less lidar measurements.

Importantly, the same trend calculation based on the lidar data between 2000 and 2018 is conducted in this study as well to investigate the mesopause trend without the potential effect of Mt. Pinatubo eruption. This trend calculation reveals that while the decreasing a mesopause heights (470 ± 160 m/decade for HM and 150 ± 290 m/decade for LM) is consistent and have similar magnitude to those derived from the 29-year lidar data but with larger uncertainties, the cooling trends for both LM (1.0 ± 0.9 K/decade) and HM (0.2 ± 0.7 K/decade) become considerably less. Therefore, considering the uncertainty (one sigma), since 2000 when the Mt. Pinatubo effect is believed to become marginal, the temperature of either LM or HM demonstrates either no trend or a considerable less cooling trend than that derived from all of the lidar measurements between 1990 and 2018. This analysis also confirms the fact that though the episodic warming in the 1990s produced a larger cooling trend, it does not impact the long-term trend in LM and HM heights.

In addition, we have also tested the sensitivity of the 29-year trend results by setting different height limit of LM and HM in the regression process. While the cooling trends of LM and HM are fairly robust, the change of height limit does slightly affect the height trend. For example, changing the upper limit of LM to 94 km, its cooling trend stays almost the same as 2.4 ± 0.5 K/decade within the uncertainty. Meanwhile, its height downward trend becomes 310 ± 180 m/decade. The same test was conducted by setting lower limit of HM to 99 km, and similar results are achieved for both the temperature and height trends (cooling of 2.5 ± 0.5 K/decade and downward 430 ± 80 m/decade). This test demonstrates the robustness of our algorithm in this long-term investigation.

Categorizing the lidar measured mesopause differently based solely on seasons (summer/winter), height, and the combination of the two (summer LM/winter HM), we conducted the same trend calculation to see how sorting the lidar data differently affects the trend results. Considering the changing fitting uncer- tainties in different approach, the overall long-term mesopause trend results are fairly similar with decreas- ing the HM height of a few hundred meters per decade and cooling mesopause temperature. These results also confirm that the decreasing of the LM height is not evident and there is no clear trend of mesopause
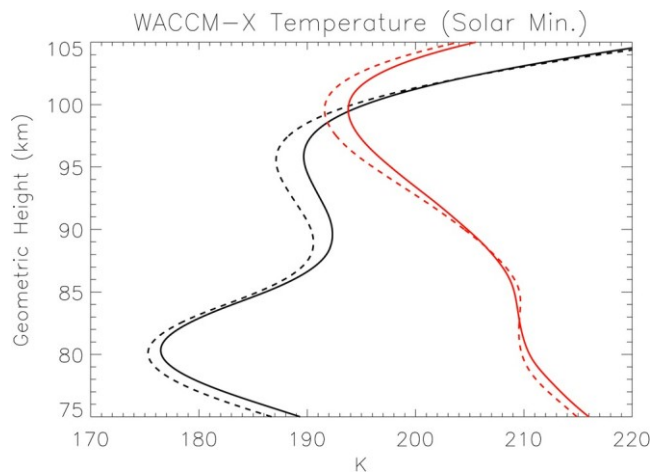
Figure 5. Whole Atmosphere Community Climate Model with thermosphere and ionosphere extension (WACCM-X; 2.0) simulated summer temperature profiles for the years 1972-1976 (black solid line) and the years 2001-2005 (black dashed line); winter temperature profiles of 1972-1976 (red solid line) and 2001-2005 (red dashed line). Both epochs were run with lower boundary conditions (particularly anthropogenic inputs) representative of those periods, but with constant solar and geomagnetic forcing, assuming solar minimum conditions.

since 2000 within the uncertainty for both kinds of mesopause, except the dropping of the HM height. Note that the trend results based solely on height of mesopause (<92 km for LM and >97 km for HM) are almost identical to those based on height and seasons that we are currently focusing on in this investigation. These results are listed in Appendix A.

3. Long-Term Mesopause Trends Simulated by WACCM-X

The recent WACCM-X (2.0) simulation under solar minimum conditions (F10.7 = 70) by Solomon et al. (2018) indicates a small cooling trend of zonal mean temperature in the middle latitude mesopause region, ~1 K/decade, while the thermosphere has the largest response, -2.8 K/decade, and atmospheric density decrease of ~4%/decade at 400-km altitude. WACCM-X v. 2.0 is currently based on National Center for Atmospheric Research Community Atmosphere Model (CAM-4) physics, as released in Community Earth System Model (CESM) 1.0 (Hurrell et al., 2006; Neale et al., 2013), and employs a conventional latitude-longitude grid with horizontal resolution of 1.9° in latitude and 2.5° in longitude. The default vertical resolution is the same as WACCM below 0.96 hPa but has been increased to one-quarter scale height above that pressure level. The long-term simulation was conducted for two 5-year periods: 1972 to 1976 and 2001 to 2005, using constant solar and geomagnetic forcing under solar minimum conditions. It is worth noting that this set up skips the period when Mt. Pinatubo eruption was affecting the global atmosphere in the 1990s. Thus, this set of trend results are not affected by this volcano effects. For more details on the model simulations see Solomon et al. (2018) and Liu et al. (2018).

The long-term effects are derived by computing monthly averages of each 5-year ensemble at every grid point, at which the trends are obtained. These are designated as "1974" and "2003," respectively, in the following text. Here the monthly averaged model outputs at the grid point closest to the lidar station (40.7°N, 105°W) are employed to provide a reference for the theoretical trend of the midlatitude mesopause. The nonwinter "LM" is derived by averaging the results for May-June-July, and the nonsummer "HM" is obtained by averaging the results for November-December-January-February.

Unlike lidar summer measurements (where about 9% of the nights have mesopause above 97 km), the summer mesopause (May-July) in the simulations are all LM. The heights of the winter mesopause (November-February) are all above 97 km. Thus, their trends can be characterized as those of LM and HM, and directly compared with the trends of the lidar-measured nonwinter LM and nonsummer HM. Figure 5 shows the WACCM-X (2.0) averaged temperature profiles near CSU/USU lidar station for summer and winter for year 1974 and 2003 under perpetual solar minimum condition based on the sampling of all UT time. The trend is derived by calculating the difference in mesopause height and temperature between the two averaged profiles for summer and winter, respectively, and dividing the difference by 29 years. Since the model is running in pressure level, the mesopause height is identified first at the pressure level where the minimum temperature occurs. Then, the associated geometric height is treated as the altitude of the mesopause. The model outputs between 70 and 120 km are interpolated onto a high-resolution grid and, using cubic spines, the temperature minima can be accurately identified. The winter mesopause in the model occurs at the same pressure level in the 1974 profile as that of 2003 (3.8e-4 hPa), the associated geometric heights are 99.613 and 99.094 km, respectively. Thus, the simulated winter mesopause, or HM, shows a downward trend of 179 m/decade. This simple calculation also shows that the winter mesopause in WACCM-X (2.0) has a cooling trend as well, 0.75 K/decade. For the summer mesopause (LM) in the model simulation, the pressure level is 7.7e-3 hpa for the two profiles, and the mesopause temperature and height trends are -0.41 K/decade and -230 m/decade, respectively, which are similar to those of the simulated HM. Compared with the lidar-measured trends, the cooling trend revealed by the model simulation is considerably less than those based on 29-year lidar run, but similar to the statistically insignificant lidar trend after 2000. The model

results also demonstrate decreasing of mesopause height with similar magnitude as those revealed by the lidar observations.

4. Discussion

The reported decrease of mesopause height is expected, due to contraction of the stratosphere-mesosphere, as pressure levels move down to lower altitude. Lübken et al. (2013) comprehensively simulated the summer mesospheric temperature trend at midlatitude by using Leibniz-Institute Middle Atmosphere model driven by European Centre for Medium-Range Weather Forecasts reanalysis below approximately 40 km and adapts temporal variations of CO_2 and O_3 according to observations. They have also revealed the summer 92-km pressure height decreased by ~300 m between 1991 and 2009 and ~600 m between 1974 and 2003 (Figure 12 in Lübken et al., 2013), which is in similar order of magnitude to the LM height trend results from the lidar measurements and those from WACCM-X (2.0). This is analogous to the trend of radio wave reflection heights in the ionosphere, which also approximately correspond to levels of constant electron density, and thus can indirectly reflect the trend of atmospheric shrinking (Bremer & Peters, 2008). In addition, Clemesha et al. (1997) reported centroid height of mesospheric Na layer fell 370 m/decade between 1972 and 1994, which is in the same order of magnitude to the lidar mesopause height trends as well.

The observed mesopause cooling is more or less in line with the previous MLT trend studies in the mesopause region, showing cooling in northern hemisphere (Beig, 2011). As discussed earlier, although both the model simulation and lidar observations between 1990 and 2018 indicate cooling of mesopause tempera- ture, the magnitude differs considerably. According to previous model simulations, increasing CO_2 is the pri- mary cause of stratosphere-mesosphere cooling and consequent atmospheric contraction, while the roles of the other species, such as O_3 and CH_4 and volcano effect can also be significant (Garcia et al., 2007; Laštovička, 2012; Laštovička & Bremer, 2004; Laštovička, Solomon, et al., 2012; Qian et al., 2013, and the references within). The cooling trend of the upper mesosphere can be attributed to increasing radiative cool- ing due to accumulation of CO_2 and the stratosphere-mesosphere contraction, which guides the large nega- tive temperature vertical gradient to lower altitude, causing cooling temperature at a specific geometric altitude in upper mesosphere. However, as demonstrated in WACCM-X simulations, the mesopause stays at an approximately static pressure level in winter, and at another pressure level at lower altitude in summer. Therefore, its winter nighttime cooling trend should be mostly contributed by the increasing radiative cool- ing. The lidar-measured HM, occurring between late fall and early spring, behaves quite similar to the winter mesopause and, thus, should be dominated by radiative cooling as well. In addition to the long-term change of CO_2 radiative cooling, in summer time, when the LM occurs, the mesopause temperature is greatly con- trolled by the adiabatic cooling due to the up-welling flow, making its temperature trend more complicated than that of the HM.

The distinct mechanisms between LM and HM can contribute to their different response to solar flux. As mentioned earlier, the height trend of the LM, which has a slight anticorrelation to the solar flux variation, is found to be more sensitive to solar flux than that of the HM. Indeed, the lidar data also demonstrate that the LM temperature response to solar flux (0.03 ± 0.1 K/SFU) is considerable larger than that of HM (0.01 ± 0.007 K/SFU) by a factor of about 3, while, as we state earlier, the LM height response to solar flux (-120 ± 30 m/SFU) is also roughly 100 times larger than that of HM height (1 m/SFU). These results could implicate that the solar flux variation affects the steady state global atmospheric circulation and, thus, the associated vertical adiabatic flow, which causes the different response to solar flux between the LM and the HM.

The effects of solar activity variation on climate and atmosphere below mesosphere have been well docu- mented by Gray et al. (2010) and the references within). The mechanisms include the atmospheric response to the changing of solar irradiance and the energetic particles, such as those during solar energetic particle events, both of which can induce circulation variations in the upper atmosphere. This may explain the lidar observed stronger solar flux index of the LM, which is mostly controlled by the adiabatic circulation, com- pared to the HM. Indeed, the evidence of MLT temperature response to solar activity is recently revealed by the lidar observations (Yuan et al., 2015) and the associated studies by the recent Thermosphere Ionosphere Mesosphere Electrodynamics General Circulation Model (TIME-GCM) simulation during a cor- onal mass ejection event (Li et al., 2018). These studies have demonstrated the change of adiabatic flow in

middle latitude MLT during these extreme solar events, which induced the corresponding temperature enhancement in the upper atmosphere.

While demonstrating similar mesopause height trend to the lidar observations, the considerably less cooling in the model results are not unexpected. The WACCM-X results are multiyear averaged based on both day and night output, the temperature change also has a contribution from absorption of solar UV radiation and associated exothermic reactions, which dominate the daytime energy budget (mainly exothermic heating from atomic Oxygen recombination (Brasseur & Solomon, 2005). These heating processes could balance the radiative cooling in the mesopause region, generating a relatively small cooling trend. The two sets of data are looking at different periods (WACCM-X covers 1974-2003, the Na lidar covers 1990-2018), which could have different trends during changing in stratosphere-mesosphere contraction (Berger & Lübken, 2011). Finally, current long-term analysis on mesopause ignores the effects of Mt Pinatubo eruption in June 1991. As we mentioned earlier, this volcano effect is also excluded in this WACCM-X model long-term trend study. However, due to the complexity of this volcano effects in MLT, the lidar-observed 29-year cool- ing trend may still have traces of its contribution, which is also possible even for the data set after 2000. She et al. (2009) compared the trends with and without Mt. Pinatubo effect based on 18 years of lidar data (1990-2007) and discovered that the inclusion of the volcano impact, through a nonlinear response function, reduces the cooling trend in the mesopause region considerably. Indeed, although with larger uncertainties, the lidar observations reveal that the mesopause temperature cooling trends for both HM and LM after 2000, when this volcano effect is believed to become insignificant, are much less than those derived based on the overall 29-year lidar observations. Thus, precisely charactering this volcano response term in the analysis, along with its inclusion in the regression algorithm, may lead to less cooling of mesopause temperature (She et al., 2009).

5. Conclusions

The CSU/USU Na lidar nocturnal temperature observations between 1990 and 2018 provide the longest continuous multidecade neutral temperature data base in MLT. In this study, taking advantage of this data set, we investigated the long-term trend of an important upper atmosphere boundary between mesosphere and thermosphere, the mesopause, who has the coldest temperature in Earth atmosphere. We derived trends of mesopause temperature and height to understand the magnitude of upper mesosphere cooling and long‐term pace of atmospheric contraction. The lidar-measured nocturnal mesopause data are categorized into nonwinter LM (occurring in late spring and summer) and nonsummer HM (fall to early spring), which are controlled mostly by the adiabatic cooling and radiative cooling, respectively. To our knowledge, this is the first long-term trend study on the mesopause. Because the mesopause occurs at specific pressure level, the stratosphere-mesosphere contraction has quite limited impact on its temperature trend in the pressure unit.

The lidar results demonstrate a downward trend of 450 ± 90 m/decade and cooling trend of 2.5 ± 0.4 K/decade for the HM, a slower downward trend of 130 ± 160 m/decade and similar 2.3 ± 0.5 K/decade cooling trend for the LM from 1990 to 2018. The trend analysis based on lidar data since 2000 reveal considerably less mesopause cooling trend (<1 K/decade) with slightly larger uncertainty, but the trends of mesopause height are consistent (470 ± 160 m/decade for HM and 150 ± 290 m/decade for LM). The lidar data also revealed that the trend of the LM height is quite sensitive to solar flux and anticorrelated to solar cycle effect (-120 ± 30 m/SFU), while the HM height has very little response to solar flux F10.7 (1 m/SFU). The asso‐ ciated mesopause temperature trend also indicates LM has larger response to solar flux variation (0.03 ± 0.1 K/SFU) than HM does (0.01 ± 0.007 K/SFU). This is likely due to fact that the LM is mostly controlled by the dynamic processes (adiabatic vertical flow), which are prominent in MLT and are sensitive to solar activity. These lidar results, except those of solar flux response, are compared with the recent long-term trend study by WACCM-X that simulated the atmosphere change between 1974 and 2003 (Solomon et al., 2018). While the cooling trend of mesopause temperature and downward trend of mesopause height are confirmed, the magnitude of mesopause cooling in this model simulation (less than 1 K/decade) is significantly smaller than the lidar measured 29-year trend results, but in line with the lidar revealed trend after 2000 when the effect of Mt. Pinatubo eruption is believed to become insignificant. The long-term trend of tidal wave could also play some role in our trend results.

The uncertainty of the regression algorithm on lidar mesopause height is still relatively large, especially for the LM that has less than half of the data points of the HM. Therefore, more observations between April and early August should be planned in the future to balance the statistic uncertainty. At the same time, a comprehensive quantification of Mt. Pinatubo effect in MLT and its inclusion in the lidar data regression are also necessary to provide more solid trend results, as hinted by the analysis using the lidar data after 2000. Future work will also entail a long-term continuous model run, with high-frequency output, to enable the simulation to be analyzed in the same way as the lidar data.

Appendix A

To investigate the effects of different ways of data sorting on the trend results, here, we present the lidar trend results based on four different sorting algorithms for the 29-year lidar data (1990-2018) and for the later 19-year lidar data (2000-2018), along with the number of nights in each of the category:

The Mesopause Trend Results Based on Different Approaches of Data Sorting

1990-2018				
Summer/winter (no. of nights 359/391)				
Trend_Temperature (K/dec.)			Trend_Height (m/dec.)	
WM	-4	0.7	-280	230
SM	-1.6	0.5	230	350
Height only (no. of nights 398/884)				
Trend_Temperature (K/dec.)			Trend_Height	
HM	-2.5	0.4	-430	90
LM	-2.7	0.6	-230	160
Height (non winter LM/non summer HM: no. of nights 388/824)				
Trend_Temperature (K/dec.)			Trend_Height	
HM	**-2.5**	**0.4**	**-450**	**90**
LM	**-2.3**	**0.5**	**-130**	**160**
Height (winter HM/summer LM: no. of nights 304/359)				
Trend_Temperature (K/dec.)			Trend_Height	
HM	-3.8	0.7	-620	150
LM	-1.75	0.5	10	180
2000-2018				
Summer/winter (no. of nights 256/242)				
Trend_Temperature (K/dec.)			Trend_Height (m/dec.)	
WM	0.1	1	-840	380
SM	-0.3	0.9	410	620
Height only (no. of nights 271/595)				
Trend_Temperature (K/dec.)			Trend_Height	
HM	-0.4	0.6	-420	150
LM	-1	0.9	120	290
Height (nonwinter LM/nonsummer HM: no. of nights 268/556)				
Trend_Temperature (K/dec.)			Trend_Height	
HM	-0.2	0.7	-470	160
LM	-1	0.9	150	290
Height (winter HM/summer LM: no. of nights 212/225)				
Trend_Temperature (K/dec.)			Trend_Height	
HM	-0.2	1	-680	260
LM	-1.5	0.9	360	330

Note. The values in bold are presented in the paper as the final results.

1. summer (May - July) mesopause and winter (November - February) mesopause;
2. height only: low mesopause (<92 km) and high mesopause (>97 km);
3. nonwinter low mesopause and nonsummer high mesopause; and
4. Summer low mesopause and winter high mesopause

References

Akmaev, R. A., Fomichev, V. I., & Zhu, X. (2006). Impact of middle-atmospheric composition changes on greenhouse cooling in the upper atmosphere. *Journal Atmosphere and Solar: Terrestrial Physics*, *68*(17), 1879–1889. https://doi.org/10.1016/j.jastp.2006.03.008

Beig, G. (2011). Long-term trends in the temperature of the mesosphere/lower thermosphere region: 1. Anthropogenic influences. *Journal of Geophysical Research*, *116*(A2), A00H11. https://doi.org/10.1029/2011JA016646

Berger, U., & Lübken, F.-J. (2011). Mesospheric temperature trends at mid-latitudes in summer. *Geophysical Research Letters*, *38*, L22804. https://doi.org/10.1029/2011GL049528

Brasseur, G. P., & Solomon, S. (2005). *Aeronomy of the middle aatmosphere: Chemistry and physics of the stratosphere and mesosphere*. New York: Springer. https://doi.org/10.1007/1-4020-3824-0

Bremer, J., & Peters, D. (2008). Influence of stratospheric ozone changes on long-term trends in the meso- and lower thermosphere. *Journal Atmosphere and Solar: Terrestrial Physics*, *70*(11-12), 1473–1481. https://doi.org/10.1016/j.jastp.2008.03.024

Clemesha, B. R., Batista, P. P., & Simonich, D. M. (1997). Long-term and solar cycle changes in the atmospheric sodium layer. *Journal of Atmospheric and Solar: Terrestrial Physics*, *59*(13), 1673–1678. https://doi.org/10.1016/S1364-6826(96)00166-6

Garcia, R. R., Marsh, D. R., Kinnison, D. E., Boville, B. A., & Sassi, F. (2007). Simulation of secular trends in the middle atmosphere, 1950–2003. *Journal of Geophysical Research*, *112*(D9), D09301. https://doi.org/10.1029/2006JD007485

Gray, L. J., Beer, J., Geller, M., Haigh, J. D., Lockwood, M., Matthes, K., et al. (2010). Solar influences on climate. *Reviews of Geophysics*, *48*, RG4001. https://doi.org/10.1029/2009RG000282

Holton, J. R. (1983). The Influence of Gravity Wave Breaking on the General Circulation of the Middle Atmosphere. *Journal of the Atmospheric Sciences*, *40*(10), 2497–2507. https://doi.org/10.1175/1520-0469(1983)040<2497:TIOGWB>2.0.CO;2

Hurrell, J. W., Hack, J. J., Phillips, A. S., Caron, J., & Yin, J. (2006). The dynamical simulation of the Community Atmosphere Model version 3 (CAM3). *Journal of Climate*, *19*, 2162–2183.

Krueger, D. A., She, C.-Y., & Yuan, T. (2015). Retrieving mesopause temperature and line-of-sight wind from full-diurnal-cycle Na lidar observations. *Applied Optics*, *54*(32), 9469–9489. https://doi.org/10.1364/AO.54.009469

Laštovička, J. (2012). On the role of ozone in long-term trends in the upper atmosphere-ionosphere system. *Annales de Geophysique*, *30*(5), 811–816. https://doi.org/10.5194/angeo-30-811-2012

Laštovička, J., & Bremer, J. (2004). An overview of long-term trends in the lower ionosphere below 120 km. *Journal Surveys in Geophysics*, *25*(1), 69–99. https://doi.org/10.1023/B:GEOP.0000015388.75164.e2

Laštovička, J., Solomon, S. C., & Qian, L. (2012). Trends in the neutral and ionized upper atmosphere. *Space Science Reviews*, *168*(1-4), 113–145. https://doi.org/10.1007/s11214-011-9799-3

Li, J., Wang, W., Lu, J., Yuan, T., Yue, J., Liu, X., et al. (2018). On the responses of mesosphere and lower thermosphere temperatures to geomagnetic storms at low and middle latitudes. *Geophysical Research Letters*, *45*(19), 10,128–10,137. https://doi.org/10.1029/2018GL078968

Liu, H.-L., Bardeen, C. G., Foster, B. T., Lauritzen, P., Liu, J., Lu, G., et al. (2018). Development and validation of the Whole Atmosphere Community Climate Model with thermosphere and ionosphere extension (WACCM-X 2.0). *Journal of Advances in Modeling Earth Systems*, *10*(2), 381–402. https://doi.org/10.1002/2017MS001232

Lübken, F.-J., Berger, U., & Baumgarten, G. (2013). Temperature trends in the midlatitude summer mesosphere. *Journal of Geophysical Research: Atmospheres*, *118*, 13,347–13,360. https://doi.org/10.1002/2013JD020576

Neale, R., Richter, J., Park, S., Lauritzen, P., Vavrus, S., Rasch, P., & Zhang, M. (2013). The mean climate of the Community Atmosphere Model (CAM4) in forced SST and fully coupled experiments. *Journal of Climate*, *26*(14), 5150–5168. https://doi.org/10.1175/JCLI-D-12-00236.1

Qian, L., Marsh, D., Merkel, A., Solomon, S. C., & Roble, R. G. (2013). Effect of trends of middle atmosphere gases on the mesosphere and thermosphere. *Journal of Geophysical Research: Space Physics*, *118*, 3846–3855. https://doi.org/10.1002/jgra.50354

Roble, R. G. (1995). Energetics of the mesosphere and thermosphere. In R. M. Johnson & T. L. Killeen (Eds.), *The upper mesosphere and lower thermosphere: A Review of Experiment and Theory, Geophysical Monograph Series* (Vol. 87, pp. 1–21). Washington, DC: American Geophysical Union.

Roble, R. G., & Dickinson, R. E. (1989). How will changes in carbon dioxide and methane modify the mean structure of the mesosphere and thermosphere. *Geophysical Research Letters*, *16*(12), 1441–1444. https://doi.org/10.1029/GL016i012p01441

She, C. Y., Krueger, D. A., Akmaev, R., Schmidt, H., Talaat, E., & Yee, S. (2009). Long-term variability in mesopause region temperatures over Fort Collins, Colorado (41°N, 105°W) based on lidar observations from 1990 through 2007. *Journal of Atmospheric and Solar: Terrestrial Physics*, *71*(14–15), 1558–1564. https://doi.org/:10.1016/j.jastp.2009.05.007

She, C.-Y., Krueger, D. A., & Yuan, T. (2015). Long-term midlatitude mesopause region temperature trend deduced from quarter century (1990–2014) Na lidar observations. *Annales de Geophysique*, *33*(3), 363–369. https://doi.org/10.5194/angeo-33-363-2015

She, C. Y., & von Zahn, U. (1998). The concept of two-level mesopause: Support through new lidar observation. *Journal of Geophysical Research*, *103*(D5), 5855–5863. https://doi.org/10.1029/97JD03450

She, C. Y., Yu, J. R., & Chen, H. (1993). Observed thermal structure of a midlatitude mesopause. *Geophysical Research Letters*, *20*(7), 567–570. https://doi.org/10.1029/93GL00808

Solomon, S. C., Liu, H.-L., Marsh, D. R., McInerney, J. M., Qian, L., & Vitt, F. M. (2018). Whole atmosphere simulation of anthropogenic climate change. *Geophysical Research Letters*, *45*(3), 1567–1576. https://doi.org/10.1002/2017GL076950

von Zahn, U., Höffner, J., Eska, V., & Alpers, M. (1996). The mesopause altitude: only two distinctive levels worldwide? *Geophysical Research Letters*, *23*(22), 3231–3234. https://doi.org/10.1029/96GL03041

Xu, J., Liu, H.-L., Yuan, W., Smith, A. K., Roble, R. G., Mertens, C. J., et al. (2007). Mesopause structure from Thermosphere, Ionosphere, Mesosphere, Energetics, and Dynamics (TIMED)/Sounding of the Atmosphere Using Broadband Emission Radiometry (SABER) observations. *Journal of Geophysical Research*, *112*, D09102. https://doi.org/10.1029/2006JD007711

Yuan, T. (2018). USU Na Lidar Data. Browse all Datasets. Paper 54. https://digitalcommons.usu.edu/all_datasets/54

Yuan, T., She, C., Krueger, D. A., Sassi, F., Garcia, R., Roble, R. G., et al. (2008). Climatology of mesopause region temperature, zonal wind, and meridional wind over Fort Collins, Colorado (41°N, 105°W), and comparison with model simulations. *Journal of Geophysical Research*, *113*(D3), D03105. https://doi.org/10.1029/2007JD008697

Yuan, T., Zhang, Y., Cai, X., She, C.-Y., & Paxton, L. J. (2015). Impacts of CME-induced geomagnetic storms on the midlatitude mesosphere and lower thermosphere observed by a sodium lidar and TIMED/GUVI. *Geophysical Research Letters*, *42*, 7295–7302. https://doi.org/10.1002/2015GL064860